LAND DEGRADATION & DEVELOPMENT
Land Degrad. Develop. **28**: 2527–2539 (2017)
Published online 20 September 2017 in Wiley Online Library (wileyonlinelibrary.com) **DOI**: 10.1002/ldr.2803

FINGERPRINTING SEDIMENT SOURCES AFTER AN EXTREME RAINSTORM EVENT IN A SMALL CATCHMENT ON THE LOESS PLATEAU, PR CHINA

Jiaqiong Zhang[1], Mingyi Yang[1]*, Fengbao Zhang[1], Wei Zhang[2], Tianyin Zhao[1], Yuanyuan Li[1]

[1]*State Key Laboratory of Soil Erosion and Dryland Farming on the Loess Plateau, Institute of Soil and Water Conservation, Northwest A&F University, Yangling, Shaanxi 712100, PR China*
[2]*Agricultural Committee of Wuzhai County, Xinzhou, Shanxi 036200, PR China*

Received 5 October 2016; Revised 20 April 2017; Accepted 20 August 2017

ABSTRACT

Soil erosion is a severe problem on China's Loess Plateau due to its fine-grained soils and the increasing frequency of extreme rainfall events. Accordingly, this study used a 100-year frequency rainstorm dataset to analyse sediment deposition and sources in a 27-km^2 catchment with a dam field area of 0·14 km^2 based on the hypothesis that sediments were intercepted by the dam (before collapse) during the rainstorm event and deposited in the dam field. This study applied composite fingerprinting, which revealed the sediment source contributions and estimated sediment deposition. Sediment deposition (626·4 kg m^{-2}) decreased linearly or exponentially with increasing distance from the dam. Composite fingerprints based on the optimal parameters revealed relative sediment contributions of 44·1% ± 25·5%, 37·7% ± 35·0%, 9·0% ± 11·4% and 9·2% ± 11·5% by bare ground, croplands, grassland and forests, respectively. The 5-year cumulative sediment deposition from normal rainfall was 2·3 × 10^4 t less than the extreme rainstorm. Bare grounds and croplands were the dominant sediment sources following both the extreme rainstorm and normal erosive rainfall events but varied at different areas of the check-dam. Erosion patterns and start times depended on land use type, thereby affecting sediment profiles in the dam field. Furthermore, severe erosion from bare ground that were all gully slopes and gully walls occurred throughout the rainfall, whereas grasslands and forest erosion occurred earlier and croplands later. Finally, extreme rainfall promoted mass wasting on slopes, gully slopes and gully walls, which are important in determining extreme rainstorm erosion pattern variation. This study aimed to reveal erosion pattern variation under extreme rainstorm events. Copyright © 2017 John Wiley & Sons, Ltd.

KEY WORDS: sediment source; sediment deposition; extreme rainstorm; check-dam; fingerprinting

INTRODUCTION

Soil characteristics greatly affect biodiversity, ecosystem services, land degradation and the security of energy, food and water supplies as well as their responses to climate change (Brevik *et al*., 2015; Smith *et al*., 2015). Soil erosion is therefore a significant threat to the provision of ecosystem services. Severe soil erosion usually operates several orders of magnitude faster than soil-formation processes (Verheijen *et al*., 2009). Thus, soil restoration takes a long time to recover after extreme erosion events. Erosion largely depends on a variety of factors, such as land use type, terrain, vegetation cover and type, inherent soil erodibility and the intensity of erosive forces (Renard *et al*., 2011; USDA, 1996). Therefore, to control soil erosion, it is important to identify the most vulnerable soils and land uses. In regions where water erosion is the dominant, studies on individual slope scale have proven fruitful (Kinnell, 2013; Li *et al*., 2009; Sun *et al*., 2013). However, only limited information is available for erosion and sediment characteristics on larger scales, such as catchments and whole river systems. Such data can highlight the importance of complex geomorphic forms on soil erosion, sediment transport and sources, as well as the important role they played in tracing the movement of sediments and their contribution to river system (Zhang *et al*., 2015; Nosrati, 2016).

Research on sediment characteristics, including their sources and yields, can clarify the physical and chemical properties of eroded soil, the potential pollutants it contains, transport and redistribution mechanisms and relationships among sediment sources, sinks and outputs in rivers or streams (Gellis & Walling, 2013; Walling, 2005). Such knowledge is important for policymakers to design suitable sediment control strategies. Although traditional methods, such as mapping, surveying, photogrammetry remote sensing and observation of erosion plots, have contributed greatly to our knowledge of soil erosion on catchment scale (Collins & Walling, 2004), such studies have important limitations. First, even though sediment yields have been defined based on observations at the outlets of catchments, this approach has spatial and temporal limitations; for example, large-scale observations over long time periods are labour-intensive and expensive. Second, sediment sources within a catchment are treated as a 'black box'; thus, it is difficult to define the relative contribution of each sediment source. Third, it is challenging to trace sediment source and yield variations in response to changes within the erosion environment over long periods, and this makes it difficult to evaluate the environmental effects.

*Correspondence to: M. Y. Yang, State Key Laboratory of Soil Erosion and Dryland Farming on the Loess Plateau, Institute of Soil and Water Conservation, Northwest A&F University, No. 26 Xinong Street Yangling, Shaanxi 712100, China.
E-mail: ymyzly@163.com

The fingerprinting technique provides an effective, direct and feasible method to trace sediment sources. This approach has been widely used to trace sources of sediments, pollutants and nutrient mobilization, as well as to estimate sediment deposition and reconstruct the deposition history of a region and its associative climate conditions (Huisman *et al*., 2013; Sukhija *et al*., 1998; Viparelli *et al*., 2013; Warren *et al*., 2003). Fingerprinting techniques have evolved from single-property fingerprints to multiproperty composite fingerprints because reliance on a single property of sediment makes it difficult to accurately distinguish sediments from a variety of sources in large fluvial systems, such as catchments (Collins & Walling, 2004). The composite fingerprint approach is principally based on three steps. The first step is to identify the potential fingerprinting properties that can distinguish the potential sediment sources from those that are statistically significant, using the Kruskal–Wallis *H* test. The second step is to classify meaningful parameters into appropriate categories by means of discriminant function analysis, which is a stepwise approach of discrimination function analysis based on Wilks's lambda distribution (Wilk's λ) that is applied when the Kruskal–Wallis *H* test cannot confirm all potential factors (Collins & Walling, 2002). The third step is to identify the optimal combination of fingerprinting properties by using multivariate discriminant analysis. This combination of fingerprinting properties is the best approach to use to distinguish between sediment sources by using the fewest properties. Composite fingerprinting is used in conjunction with a model (Gellis & Walling, 2013). The fingerprinting properties commonly used include geochemical, radionuclide, rare earth elements, magnetic susceptibility, grain size distribution of sediment and the content of various nutrient elements (Chaparro *et al*., 2015; Collins *et al*., 1997; Guzmán *et al*., 2013; Silva-Filho *et al*., 2011; Watson *et al*., 2013), and some researchers have even examined biomarkers in this context (Reiffarth *et al*., 2016). This approach makes it possible to trace the movement of drifting dust on a large scale for a long duration (Grousset & Biscaye, 2005) to clarity sources and sinks of sediment under complex topographical conditions, providing much more information than observations could yield from outlet control stations through sediment collection. Moreover, the contribution to sediment for each land use type was traced, but the total quantitative variance was not obtained. It is much more helpful to understand erosion pattern variation processes in catchments at different geomorphologic positions and for different land use types. However, it must be used carefully due to the nonconservative of sediment properties in transport processes, and the dependence of source attribution on models (Collins *et al*., 2016; Haddadchi *et al*., 2014; Koiter *et al*., 2013). Thus, the uncertainty of the approach should be assessed in application.

On China's Loess Plateau, previous research applied fingerprinting techniques to study both ancient and contemporary sediment deposits. Paleoreconstructions have included environmental and climate changes and the provenance of the Plateau's enormous deposits of loess soil (Bird *et al*., 2015; Ding *et al*., 2001; He *et al*., 2013). In contrast, contemporary studies have mainly focused on the origins of aeolian dust as well as its transport and deposition mechanisms (Cao *et al*., 2008; Jia *et al*., 2011), while also focusing on the sediment sources and yields and their implication on environmental evaluations (Long *et al*., 2012; Wang *et al*., 2016; Zhao *et al*., 2015). Although existing reports have focused on the latter aspect, such reports remain limited. This approach is suitable for this study because principle assumptions have been satisfied, which include the sediments from different potential distinguishable sources (different land use types) and stable and detectable potential fingerprint properties to resolve sediment sources problems (Koiter *et al*., 2013).

Check-dams are believed to be one of the most effective ways in reducing the volume of coarse sediments entering into a river on the Loess Plateau (Zhao *et al*., 2016). Furthermore, impounded sediment behind check-dams is far better for studying sediment transport in catchments. Sediment deposited in dam fields accurately records the catchment's soil erosion history by intercepting eroded soil transported from regions upstream of the dam field (Wei *et al*., 2017). By 2013, $0{\cdot}58 \times 10^6$ check-dams produced dam fields that covered an area of 927·6 km^2 on China's Loess Plateau, and another $1{\cdot}05 \times 10^6$ check-dams are planned to be completed by 2020 (Ministry of Water Resources, China, 2013).

Previous studies on sediment characteristics were mostly implemented over long periods of time (Chen *et al*., 2016; Zhao *et al*., 2015; Zheng *et al*., 2013) and therefore did not consider the effects of single erosion events, such as those produced by extreme rainstorms (Li *et al*., 2016; Xu *et al*., 2013). However, rainstorms, especially extreme rainstorm events, have caused the greatest sediment transport on the Loess Plateau owing to the fact that rainfall erosivity significantly affects soil erosion in this region (Li & Wei, 2014; Zheng *et al*., 2008). From 60% to 90% of the total annual sediment transport volume occurred during such rainstorm events (Zhou & Wang, 1992). During an extreme rainstorm event that occurred in July 2013 in the Yan'an District (where Yanchang County is located), 13,466·7 hectares of farmland were destroyed, 45,376 buildings collapsed, greater than 8,000 mass wasting episodes were observed, approximately 15·45 million people were affected, and the direct economic loss reached 1.8 billion US dollars. The main type of soil loss was wasting mass events and debris flows, which differed significantly from normal rainfall erosion processes (Huang *et al*., 2014).

Severe erosion caused by extreme rainstorm events has occurred time after time on the Loess Plateau (Li *et al*., 2016; Wang *et al*., 2016). To provide information on this relatively unstudied phenomenon, we used a single extreme rainstorm event of a long duration and recurrence interval as an example and analysed the sediment sources and yields from the event. Our objectives were (i) to quantify the sediment deposition produced by the 2013 extreme rainstorm event in a dam-controlled watershed; (ii) to trace sediment

sources; and (iii) to describe how sediment sources differed from those during normal rainfall events. The results of this study are meant to help policymakers develop plans to reduce erosion both during normal rainfall events and during those rare high-intensity extreme rainstorm events.

MATERIALS AND METHODS

Study Area

The Hujiawan catchment (from 36·47°N to 36·50°N and from 109·75°E to 109·80°E) is located in Yangchang County, approximately 37 km east of Yan'an City (Figure 1). The drainage area of this catchment is approximately 27 km^2 and supplies water to a secondary branch of the Yan River. The elevation ranges from 947 to 1300 m AMSL. The broken hilly terrain contains many deep erosion gullies with almost no vegetation (bare ground). The region is characteristic of a typical semiarid continental monsoon climate. The average annual precipitation is 565·7 mm, with high annual and interannual variations. Greater than 60% of the total precipitation falls between June and September, often in the form of high-intensity rainstorms.

Construction of the Hujiawan dam began in 1971 at the outlet of this catchment, and sediment was trapped in the dam from 1974 to 2003. The resultant dam field has been ploughed since 1999, with the main crop being corn (*Zea mays*); cultivation has been conducted yearly without fertilization. Land use types and areas in the catchment have

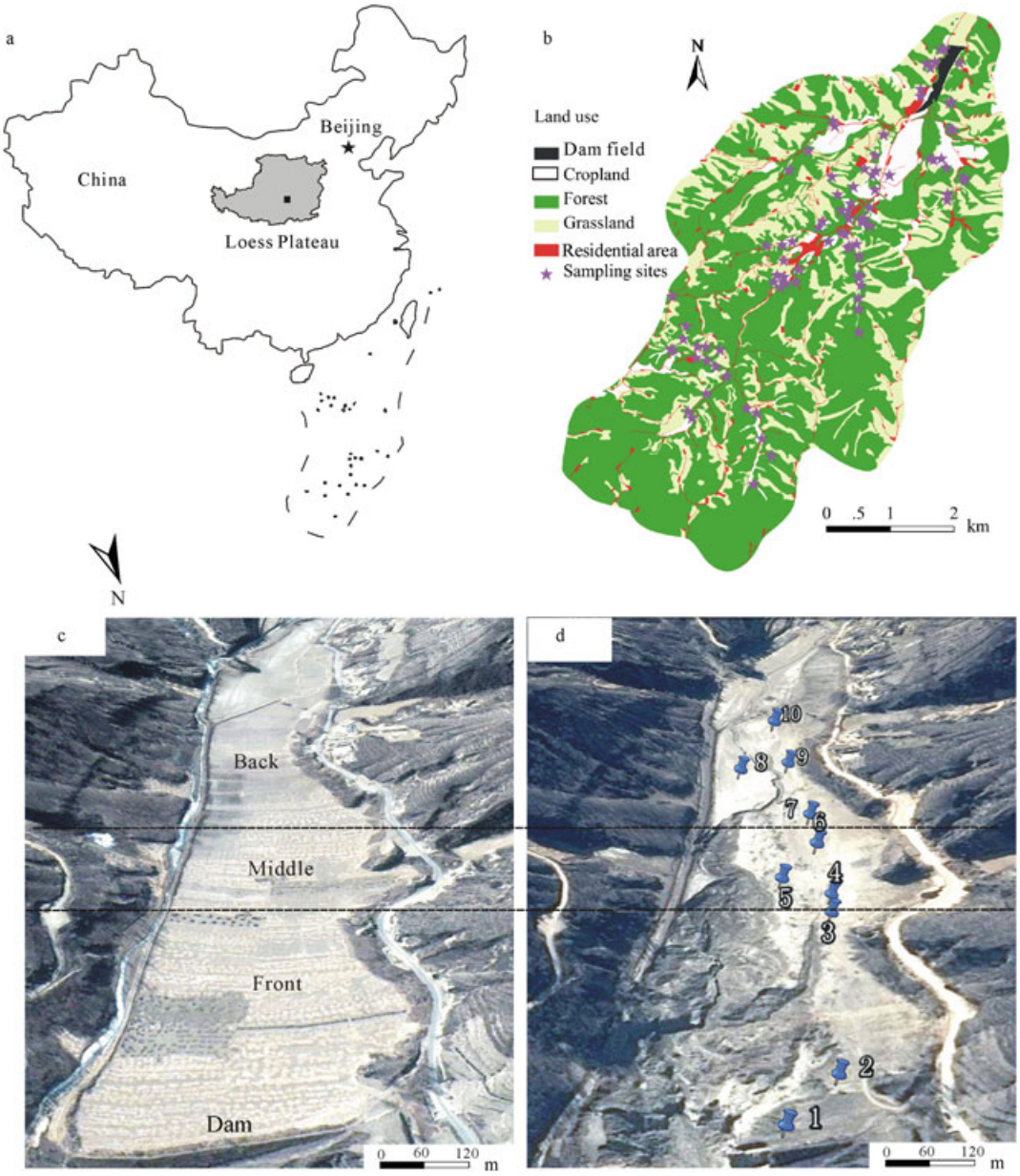

Figure 1. (a) The location of the study area, (b) map of land use types in 2010 and locations of the sampling sites within the catchment and images of the check-dam (c) before and (d) after its collapse. [Colour figure can be viewed at wileyonlinelibrary.com]

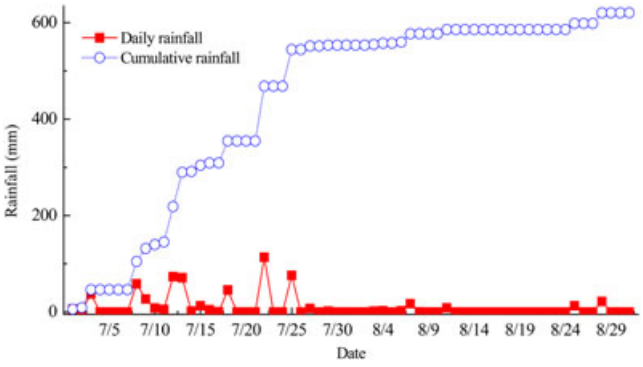

Figure 2. Rainfall from 1 July to 31 August 2013. [Colour figure can be viewed at wileyonlinelibrary.com]

changed little since the 1999 implementation of the national 'Grain for Green' programme implemented by the government of China. Under this programme, villagers were provided financial as well as other incentives to discontinue farming and livestock grazing on degraded land (particularly on slopes) and to start planting trees and grass instead.

This study selected a 100-year frequency rainstorm event that began on 1 July 2013 and continued, with some interruptions, until 29 July 2013. This was the most severe rainstorm event in the Yan'an region since 1945 and was characterized by a long duration, high intensity and high rainfall frequency. A total of 553·5 mm of rain fell during 18 days in July 2013, and another 67·1 mm fell during 8 days in August (Figure 2), and the total rainfall of this year reached 891·5 mm. It was 360·5 mm more than the mean annual precipitation during 1951 and 2012. The Hujiawan dam collapsed on 13 July 2013 after nine continuous days of rain, when the cumulative rainfall reached 289·7 mm (Table I).

Soil Sampling

Soil samples were collected both in the dam field and in the catchment. We excavated ten sampling profiles along a transect through the dam field (Figure 1d) to a depth of approximately 1 m, with the exception of the profile near to the dam (profile 1), which was sampled at a depth of 1·8 m, being dependent on thickness of the deposition layers. We first selected sampling profiles at positions with either no or only slight damage by the 2013 extreme rainstorm event, and then as close to the middle of the dam field as possible. Soil samples were collected with a wooden shovel (to avoid sediment contamination from metal ions) based on the visible variation in particle size in the vertical profile; fine and coarse layers (clay, sand, coarse sand and gravel) were collected separately. In total, we collected 109 samples, but we also used a cutting-ring sampler to collect 20 soil bulk density samples in profiles, including clay, sand, coarse sand and gravel layers (Figure 1d). Soil samples in the catchment were collected at a depth of 5 cm (i.e. surface soil) for each land use type (sloping cropland, grassland, artificial forest and bare ground). Based on the vegetation conditions, bare ground were almost always found on gully slopes and gully walls, and all bare ground samples were taken from gully slopes or walls in this study. We used a sampling depth of 5 cm in this study given that a thick layer of soil could have potentially been removed by the 2013 extreme rainfall event. Thus, this depth was better suited to represent the properties of the displaced soil, although previous studies used a sampling depth ranged from 0·5 to 5 cm (Haddadchi *et al*., 2013). We collected a total of 89 samples, of which 30 were from croplands, 20 from grasslands, 23 from artificial forests and the remaining 16 from bare ground (gully slopes or walls; Figure 1b). Three subsamples that we randomly collected from the same site were combined into a single sample. All samples were collected from 23 to 27 August 2013.

Soil Sample Analysis

All samples were air dried, ground with a mortar and pestle and passed through different size of nylon screen before determining the values of potential fingerprinting parameters: grain size distribution; soil organic matter (SOM) content; the total nitrogen, phosphorus and potassium (TN, TP and TK) contents; the magnetic susceptibility; and the contents of several geochemical elements. The potential fingerprinting properties were preliminary selected based on previous studies in this region (Chen *et al*., 2016; Xu, 2008). The particle size distribution for all particles <2 mm in diameter was determined by using a Mastersizer 2000 instrument (Malvern Instruments, Malvern, UK), and the content of particles >2 mm in diameter was determined by weighing. Based on the United States Department of Agriculture size standard (USDA, 1951); we classified particles in sediment layers into clay (<0·002 mm), silt (0·002 to 0·050 mm), fine-to-medium sand (from 0·05 to 0·50 mm), coarse sand (from 0·5 to 2·0 mm) and gravel (>2·0 mm). Silt was not

Table I. Historical rainfall data for Yanchang County for the month of July since the establishment of the weather station in 1957 (Du *et al*., 2014)

Historical July rainfall (mm)		Extreme rainfall in July	Maximum daily rainfall (mm)		Longest continuous rainfall in a year			
					Historical maximum		2013	
Average	Maximum	2013 (mm)	Historical	2013	Days	Rainfall (mm)	Days	Rainfall (mm)
119·4	304·4 (1975)	553·5	79·6 (10 July 1984)	113·6 (22 July)	12 (14–25 August 1981)	230·9	11 (8–18 July)	308·6

visually distinguishable from clay during the visual identification field sampling processes; thus, we combined them into a single clay category. However, we provided separate data for silt and clay content during the more precise particle size Mastersizer 2000 analysis procedure. SOM was determined by using the potassium dichromate external heating method. The TN content was determined by using a Kjeltec automatic nitrogen determination apparatus (Foss Instruments, Hillerod, Denmark). The TP content was determined by using the Mo-Sb colorimetric method. Soil magnetic susceptibility was measured with a Bartington MS2 dual-frequency magnetic susceptibility instrument (Bartington Instruments, Witney, UK). We tested both high-frequency (χ_{hf}) and low-frequency (χ_{lf}) susceptibilities, as well as the frequency-dependent susceptibility (χ_{fd}). The TK content and the contents of seven geochemical elements (Fe, Mn, Cu, Ca, Na, Mg and Zn) were measured by using a Z-5000 atomic absorption spectrophotometer (Thermo Instruments, Sunnyvale, CA, USA).

Sediment Deposition and Source Tracing

Distinguishing between sediment layers

We distinguished between sediment layers deposited by the extreme rainstorm and underlying layers deposited by normal rainfalls based on their properties. The top layer produced by the 2013 extreme rainstorm was defined by the presence of a visually obvious coarse layer that included coarse sand, and even some gravel above a thick tillage layer composed of homogeneous soil properties. These judgments were based on our knowledge and experience of the farming conditions in the dam field and rainfall conditions. Since 1999, this dam field has been ploughed and planted with crops, and local investigations (through interviewing local residents) have shown that it had continued to receive sediment deposition until 2003 that the check-dam was neutralized. Rainfall throughout the 5-year period was much lower compared with the 2013 rainstorm event (Table II). Therefore, a relatively homogeneous tillage layer that averaged 35·2 cm in thickness (ranging from 19 to 61 cm) was buried underneath sediments deposited by the 2013 extreme rainfall, and this layer included some crop residues. The tillage layers were formed before the extreme rainstorm, and they therefore provided a suitable control layer to identify subsequent sediment deposition. From 2003 until the collapse of the dam in July 2013, sediment did not enter the dam field and was instead discharged from the catchment through the spillway of the check-dam. However, due to the damage to the spillway (8 July 2013) and ultimate collapse of the dam (13 July 2013), sediment from the extreme rainfall event has since entered the dam field and overlaid the tillage layer.

Soil erosion was triggered by intense rainfall (>50 mm within a 24-h period) on 8, 12 and 13 July and could have been triggered by heavy rainfall (from 25 to 49·9 mm within a 24-h period) on 9 July 2013 (China Meteorological Administration, 2012; Figure 2). This intense rainstorm transported coarse particles from the slopes and gullies of the catchment into the dam field, whereby formed a layer above the tillage layer that ranged from a mixture of sand and gravel to a mixture of sand and clay. Fine particles were deposited above the coarse layer during water drainage processes before the dam collapsed. After the dam collapsed, an enormous gully up to 30 m wide and 12 m deep developed in the dam field (Figure 1d), and rainfall-driven sediments were carried away by flowing water, entering the gully after 13 July. However, because the dam field is relatively flat (with an average slope of 1·2 degree), strong rainfall after 13 July should not have transported large amounts of deposited sediment from the dam field. Therefore, we assumed that the deposition layer above the tillage layer in the dam field accurately recorded soil erosion results in the catchment starting from when the spillway was damaged on 8 July and continuing to 13 July when the dam collapsed.

Estimation of sediment deposition

Sediment deposition from the extreme rainstorm that took place from 8 to 13 July 2013 was estimated based on the soil bulk density and thickness of sediment layers at all sampling profile sites in combination with the dam field area (0·14 km^2). Deposition yields in layer i (M_i, t) were calculated as follows:

$$M_i = V_i \times \rho_i \quad (1)$$

$$M = \Sigma M_i \quad (2)$$

Table II. Rainy season rainfall from 1999 to 2003

Year	Annual rainfall (mm)	June			July			August			September		
		R (mm)	THR/TIR	MDR (mm)	R (mm)	THR/TIR	MDR (mm)	R (mm)	THR/TIR	MDR (mm)	R (mm)	THR/TIR	MDR (mm)
1999	338·4	48·3	1/0	35·5	109·8	0/0	41·9	23·3	0/0/		37·5	0/0	
2000	370·2	71·8	1/0	26·9	47·3	0/0		84.0	0/0		38·2	0/0	
2001	442·1	26·6	0/0		125·5	1/1	60·6	54·9	0/0		119·1	1/0	34·5
2002	479·8	130·7	2/0	40·9	62·6	0/0/		81·9	0/0		70·8	1/0	25·1
2003	494·0	97·3	1/0	28·0	58·4	0/0		104·2	3/1	69·9	81·4	1/0	25·2

Intense rainfall: >50 mm in 24 h, heavy rainfall: from 25 to 49·9 mm of rainfall in 24 h (China Meteorological Administration, 2012).
R, rainfall (mm); TIR ,times of intense rainfall; THR, times of heavy rainfall; MDR, max daily rainfall (mm) when intense rainfall or heavy rainfall occurred during a 1-month period.

Where: V_i is the volume of layer i (m^3); ρ_i is the bulk density of layer i (t m^{-3}); and M is the total deposition (t). We subdivided the whole check-dam field (the black area in Figure 1b) into small areas based on location of the sampling profiles. The thickness of the deposition sediment was estimated by using linear extrapolation and interpolation at various distances from each sampling point. The volumes of the layers were estimated by using version 10·0 of ARCGIS (www.esri.com) based on the area of the dam field taken from a 2010 digital elevation model in and the sediment depth in each layer. The sediment deposition of the tillage layer that formed between 1999 and 2003 was estimated by using the same procedure. Uncertainty in sediment deposition by using this method derived from the thickness estimation of the deposition sediment, given that they were depending on sampling profiles and simulated by using linearly fitting.

Sediment source tracing

We used the composite fingerprint technique in this study to trace sources of sediments produced by the extreme rainstorm event. The application of this method is based on two main assumptions: First, the potential sediment sources could be distinguished based on differences in their properties; second, the relative contribution of each potential source at a given site could be determined from the fingerprints of selected parameters (Collins & Walling, 2002). Therefore, in applying this technique, it was necessary to identify potential properties of soil in the catchment that would differ significantly between sources and deposition areas. These properties would need to remain stable during sediment transport and be measurable by using available instruments. The contribution of each potential source to sediment deposition in the dam field was ascertained by using a multivariate mixing model (Walling *et al*., 1999). This model minimizes the sum of the weighted relative square errors in a set of linear equations, and it is expressed as follows:

$$\sum_{f=1}^{n}\left\{\left[C_f-\left(\sum_{s=1}^{m}P_sS_{sf}\right)\right]/C_f\right\}^2 \tag{3}$$

Where: n is the number of fingerprinting factors selected in the optimal combination of fingerprinting factors; C_f is the concentration or value of factor f in the sediment; m is the number of potential sediment sources; P_s is the proportional contribution of sediment from potential source s; and S_{sf} is the average value of factor f in potential source s. This model was applied with two constraints: The contribution of each source is nonnegative, and contributions sum to 1 (Collins *et al*., 1997).

The source apportionment modelling outputs were tested by using artificial source material mixtures, due to the dependence of source attribution on models (Collins *et al*., 2016; Haddadchi *et al*., 2014). The uncertainty of the calculation was tested by using the goodness-of-fit (GOF), which is frequently assessed by using the relative mean error (Haddadchi *et al*., 2013),

$$\mathrm{GOF}=1-\frac{1}{n}\sum_{f=1}^{n}\frac{C_f-\sum_{s=1}^{m}x_sa_{fs}}{C_f} \tag{4}$$

Where: a_{fs} is the mean concentration of tracer property f in source type s (s = 1 to m), x_s is the unknown relative weighting contribution of source type s to the sediment sample, and C_f is the range of tracer property f in the dataset, which is used to normalize the tracer properties ranges. This equation must also satisfy the following constraints (Palazón *et al*., 2015):

$$C_f=\sum_{s=1}^{m}x_sa_{fs}, \tag{5}$$

$$\sum_{s=1}^{m}x_s=1\ \ (0\le x_s\le 1) \tag{6}$$

When the GOF value was greater than 80%, estimations of the mixing model were considered satisfactory to the contribution of sediment sources (McKinley *et al*., 2013).

RESULTS

Testing Source Apportionment Outputs of the Applied Model

The source apportionment modelling outputs were tested by using artificial source material mixtures. The preparation and testing of mixture samples were taken from source samples collected from the catchment. One sample was stochastically selected from the source samples of each land use type. They were mixed to create three types of proportional artificial mixtures: The three proportions of cropland, grassland, forest and bare ground were 1:1:1:1, 2:1:1:2 and 4:2:1:3, respectively. The multivariate mixing model was analysed with these 15 artificial mixtures. The procedure used in this study was similar to the procedure used by Haddadchi *et al*. (2014). Results showed that the cumulative classification correctness output of the multivariate mixing model was 96·6% (Tables III and IV). This means that the

Table III. Results from the Kruskal–Wallis H test for the artificial mixture samples

Element	H-value	p-value
SOM	7·740	0·021*
TN	8·525	0·038*
TP	9·084	0.011*
TK	10·140	0·006*
Cu	11·063	0·004*
Zn	10·245	0·006*
Ca	10·260	0·006*
Mg	9·260	0.100*
Na	8·420	0·015*
Fe	9·260	0.100*
Mn	9·260	0.100*
χ_{fd}	8·060	0·180*
χ_{lf}	8·780	0·120*
χ_{hf}	9·211	0.100*

*Significant at a level of a = 0·05.

Table IV. Optimal fingerprinting properties based on discrimination results of the artificial mixture samples

Step	Selected fingerprinting property	Cumulative correct classification of the source (%)	Correct classification of the source based on a single fingerprinting property (%)
1	TN	66·7	66·7
2	Fe	80·0	80·0
3	TP	91·5	86·7
4	Ca	96·6	80·0

source apportionment outputs by the applied multivariate mixing model were acceptable for this study.

Sediment Deposition Caused by the 2013 Extreme Rainstorm Event

Sediment particle size distribution varied between dam field areas (Figure 3). The deposition layers were composed of clay and sand at approximate distances less than 400 m from the dam, and coarse sand began to appear at distances from 400 to 650 m from the dam. Thick gravel layers (an average of 9·0 cm) first appeared at distances greater than 650 m from the dam, and there was almost no clay deposited at these distances. There were three obvious pairs of fine and coarse layers in sampling profiles no further than 500 m from the dam after the 2013 extreme rainstorm event (from 8 to 13 July). This means that the check-dam intercepted at least three erosion deposition events during the extreme rainstorm event, and these events occurred on the days that experienced the heaviest rainfall (8, 9, 12 and 13 July). The sediment produced on 8 or 13 July might not have entered the dam field, which would depend on the degree of damage to the spillway and the timing of the collapse of the dam. Another possibility is that sediment was deposited on 8, 9, 12 and 13 July, although the total amount of rainfall on 9 July was 27·0 mm, which was unlikely to trigger a sediment deposition event. However, this possibility of this scenario is low, given that the rain fell nearly continuously from 8 to 9 July, and precipitation on 8 July would make soil more vulnerable to erosion on 9 July, even if the total amount of rainfall on 9 July was lower. Thus, continuous rainfall from 8 to 9 July would create one fine-coarse deposition layer.

The total sediment deposition was $8{\cdot}3 \times 10^4$ t, averaging 626·4 kg m^{-2} within the 0·14 km^2 area of the dam field. The sediment deposition decreased linearly ($R^2 = 0{\cdot}919$) or exponentially ($R^2 = 0{\cdot}920$) with increasing of distance from the dam (Figure 4). The decrease was most evident within 500 m from the dam. If the dam field was divided into two regions at this distance, the sediment deposition would then decrease at average rates of 121·7 and 16·0 kg m^{-2} per 100 m, respectively.

Sources of Sediment Produced During the 2013 Extreme Rainstorm Event

Table V summarizes the values of the 14 parameters analysed to determine sediment sources. The Kruskal–Wallis *H* test showed that 11 out of the 14 parameters were potential fingerprinting properties: SOM, TN, TP, Zn, Ca, Mg, Fe, Mn, χ_{fd}, χ_{lf} and χ_{hf}. Further stepwise discriminant function analysis identified the final optimal fingerprints based on TN, Fe, TP and Ca (Table VI), with a cumulative sediment source classification correctness of 92·1% when potential sediment sources were classified into bare ground, cropland, grassland and forest.

The GOF of all the samples ranged from 86·2% to 98·5%, with an average of 93·2% ± 5·2%, which means that the mixing model algorithm approach provided acceptable predictions to the contributions of the sediment sources in the catchment (McKinley *et al*., 2013). The mean relative contributions of bare ground, croplands, grasslands and forests to dam field sediments during the extreme rainstorm event were 44·1% ± 25·5%, 37·7% ± 35·05%, 9·0% ± 11·4% and 9·2% ± 11·5%, respectively. This suggests that bare ground and croplands were the main sources, whereas grasslands and forests contributed relatively small amounts of sediment. Across the dam field, the contribution of sediment mainly derived from the bare ground and croplands in most

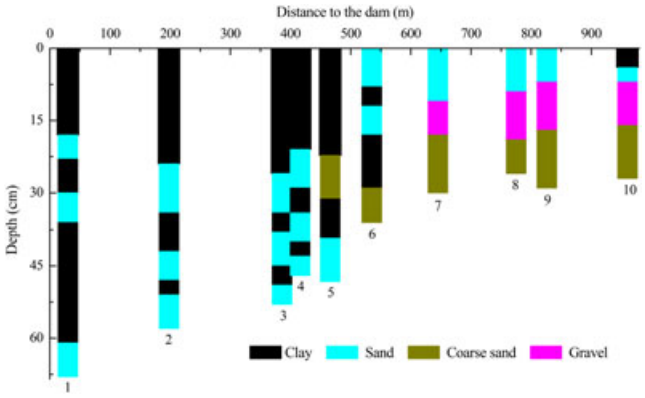

Figure 3. Sediment deposition layers that formed in the dam field after the extreme rainstorm from 8 to 13 July. Locations of the dam field sampling profiles are shown in Figure 1d. Clay, sand, coarse sand and gravel layers were identified visually in the field at the time of sampling. [Colour figure can be viewed at wileyonlinelibrary.com]

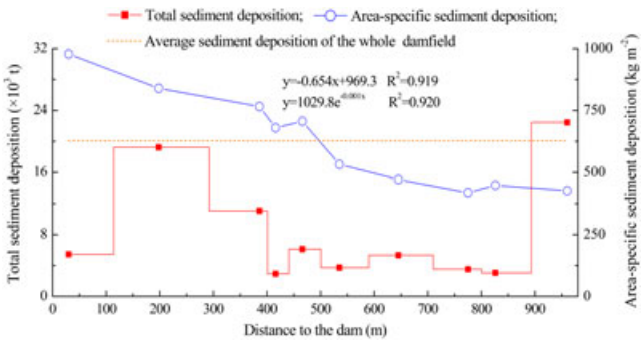

Figure 4. Sediment yield in the dam field after the extreme rainstorm. In the calculation, we used mean soil bulk densities of 1·69 g cm^{-3} for the coarse gravel layer, 1·49 g cm^{-3} for the sand layer, 1·58 g cm^{-3} for the coarse sand layer and 1·42 g cm^{-3} for the clay layer. [Colour figure can be viewed at wileyonlinelibrary.com]

Table V. Results of the Kruskal–Wallis *H* test

Element	Value[a] in source samples			Value[a] in sediment samples			*H*-value	*p*-value
	Mean	Max	Min	Mean	Max	Min		
SOM	10·66	27·66	1·99	9·48	18·03	3·88	65·927	<0·001*
TN	0·06	0·15	0.01	0·05	0·09	0.01	64·294	<0·001*
TP	0·60	0·72	0·53	0·49	0·72	0·23	8·014	0·046*
TK	17·99	20·05	14·84	10·62	20·97	8·14	4·617	0·202
Cu	0·02	0·02	0.01	0·16	0·22	0·02	1·697	0·638
Zn	0·06	0·07	0·05	0·47	0·77	0·05	11·214	0·010*
Ca	30·69	42·90	11·78	19·03	35·98	13·58	26·671	<0·001*
Mg	12·15	13·61	8·47	6·48	13·36	1·60	11·794	0·008*
Na	12·84	15·19	9·06	7·16	13·91	4·65	2·978	0·395
Fe	28·80	35·06	21·58	16·39	34·20	11·73	31·723	<0·001*
Mn	11·29	15·80	8·57	6·16	13·11	1·66	18·882	<0·001*
χ_{fd}	5·77	9·97	1.01	5·23	8·53	5·80	18·705	<0·001*
χ_{lf}	5·84	13·02	1·32	5·30	5·96	1·20	12·200	0·007*
χ_{hf}	5·48	11·75	1·30	4·92	5·48	1·19	11·6307	0·009*

[a]The following units of measurement were used: % for χ_{fd} (frequency-dependent magnetic susceptibility), 10^{-4} m^3 kg^{-1} for χ_{lf} and χ_{hf} (low-frequency and high-frequency magnetic susceptibilities, respectively) and g kg^{-1} for the remaining variables.
*Significant at a level of a = 0·05.

deposition layers (Figure 5). These two land use types contributed to all deposition layers at approximate distances greater than 650 m from the dam (profiles 7 to 10), but almost all sediment was from croplands in two of these profiles (7 and 10). Although sediment from the grasslands and forests was deposited in the top layers at distances <650 m from the dam (sample profiles 1 to 6), deposition depth decreased with increasing distance from the dam. When clay layers were found in deposition pairs, sediment derived from both grasslands and forests, or else it all derived from bare ground and croplands (profiles 7 to 9). Judged from profiles 6 to 10, all coarse particles (sand, coarse sand and gravel) derived from croplands and bare ground. When we subdivide the dam field into front (profiles 1 to 3), middle (profiles 4 to 6) and back (profiles 7 to 10) sections, the sediment mainly derived from bare ground in the front area, from bare ground and croplands in the middle area and from croplands in the back area. Secondary sediment source changed from forests to croplands moving from the front area to the middle area and to bare ground at the back area of the dam field (Table VII).

These results indicated that bare ground and croplands eroded first in the catchment and subsequently became the main sources of erosion throughout the extreme rainstorm event; as a result, sediment from these two sources was deposited in deeper layers. Only a limited quantity of soil eroded from grasslands and forests, and this occurred later in the rainstorm; as a result, sediment from these two sources was concentrated in the shallower layers (Figure 3) and transported longer distances to the front of the dam field. The high contributions of sediment from bare ground and croplands also suggested the erosion patterns that occurred during the extreme rainstorm. That is to say, gully slopes or walls collapsed and supplied a large quantity of soil for transport, whereas croplands underwent severe damage in the form of landslides (Figure 6). These phenomena were observed throughout the catchment where these land types existed. Thus, gully collapse and sheet landslide were the dominate erosion patterns during the extreme rainstorm in the catchment.

Table VI. Optimal fingerprinting properties based on discrimination results

Step	Selected fingerprinting property	Cumulative correct classification of the source (%)	Correct classification of the source based on a single fingerprinting property (%)
1	TN	66·3	66·3
2	Fe	80·9	43·8
3	TP	88·8	57·3
4	Ca	92·1	42·7

Sediment Deposition for the Extreme Rainstorm Event and Underlying Tillage Layers

Our survey found a thick cumulative tillage layer that had developed between 1999 and 2003 below the sediment layers that formed by the 2013 extreme rainstorm. Total sediment deposition produced by the extreme rainstorm was much greater than the 5-year cumulative deposition generated by normal erosive rainfall events. The tillage layer had a sediment deposition of $2{\cdot}0 \times 10^4$ t (119·5 kg m^{-2}) less than the sediment deposition produced by the extreme rainstorm event (Figure 7). Variation in the sediment deposition across the dam field was similar to deposition during the extreme rainstorm. It also decreased linearly (R^2 = 0·869) or exponentially (R^2 = 0·902) with increasing of distance from the dam. The decrease in sediment per 100 m was most evident at approximate distances less than 500 m from the dam: 1213·8 kg m^{-2} within 500 m from the dam versus 23·1 kg m^{-2} beyond that distance. The sediment sources in the cumulative tillage layer were difficult to analyse in

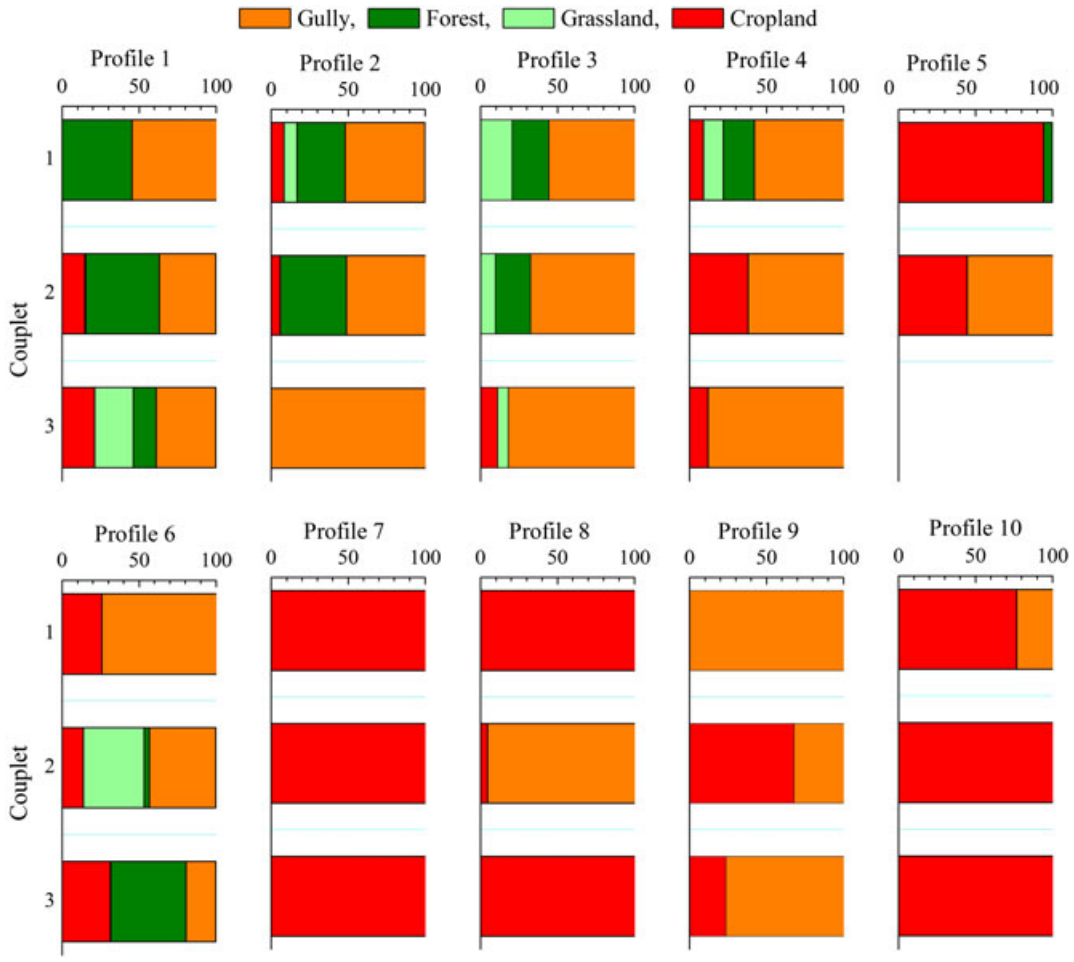

Figure 5. Contributions of the four land uses to sediment yield in the rainstorm deposition at each sample profile. Sampling depth increases with increasing couplet number. Locations of the 10 sampling profiles are shown in Figure 1d; smaller numbers represent sites closer to the dam. [Colour figure can be viewed at wileyonlinelibrary.com]

layers related to erosion events because the deposition layers had been destroyed by yearly tillage, although some thin clay or sand layers remained intact in the thick tillage layer when deposition thickness was greater than tillage depth (about 20 cm).

Sediment Sources for the Extreme Rainstorm Event and Underlying Tillage Layers

The optimal composite fingerprint parameters including TN, Fe, TP and Ca showed that the mean relative contributions of bare ground, croplands, grasslands and forests to dam field sediments for the tillage layer were 52·6% ± 12·4%, 28·7% ± 20·7%, 6·8% ± 0·6% and 12·0% ± 14·4%, respectively. Bare ground and croplands were the main sediment sources, and they exhibited similar total contributions to the sediment deposition in all layers of the dam field. However, bare ground and forests contributed less sediment during the rainstorm event than they did in the underlying tillage layer, whereas croplands and grasslands contributed more sediment. Overall, the front and middle areas of the

Table VII. Contributions of sediment from different land use types in the dam field during the 2013 extreme rainstorm as well as the underlying tillage layers

Layers	Contribution (%)											
	Profiles 1–3				Profiles 4–6				Profiles 7–10			
	C	Gr	F	BG	C	Gr	F	BG	C	Gr	F	BG
Rainstorm	7.0	12·7	22·3	58·0	37·4	13·2	3·7	45·6	61·0	3·0	3·4	32·6
Tillage	4.0	8·3	31·2	56·4	30·5	10·9	3·6	54·9	45·8	2·5	3·8	47·9

Land use types: C, cropland; Gr, grassland; F, forest; BG, bare ground. Profiles 1 to 3 represent frontal areas, 4 to 6 represent middle areas and 7 to 10 represent back areas of the dam field. Figure 1d showed their locations.

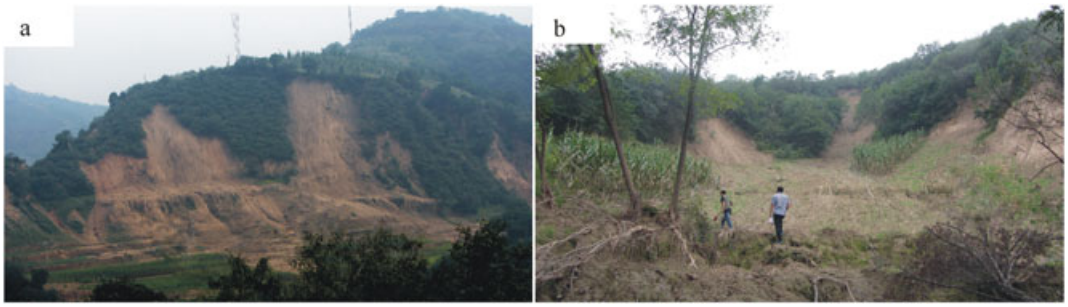

Figure 6. Examples of (a) gully collapse and (b) landslide due to slippage of surface soil in sloping cropland in the studied catchment during the rainstorm event. [Colour figure can be viewed at wileyonlinelibrary.com]

dam field showed similar sediment contributions from different sources in the rainstorm event layer and the underlying tillage layer. Bare ground were the primary sediment source, and the secondary source changed from forests in the front area of the dam field to croplands in the middle area. In the back area of the dam field, sediment mainly derived from croplands and bare ground, but bare ground were the main source for the rainstorm event layer, while both sources contributed similarly to the tillage layer (Table VII).

DISCUSSION

Soil erosion in catchments of the hilly area occurred on both slopes and in gullies. The eroded soil was transported to the outlet of the catchment and formed sediment (López-Vicente *et al*., 2015; Taguas *et al*., 2015). Depending on the type of sediment deposited in the check-dam located at the outlet of the catchment, the fingerpringting approach showed that soil loss from farmland was much greater than from grassland and forest on slopes, and this has also been widely accepted by the scientific community (Boardman *et al*., 1990; Durán-Zuazoa *et al*., 2013). Additionally, slope area contributed roughly half of the total sediment, and its contribution increased during the 2013 rainstorm event compared with normal rainfall erosion events. Contributions of sediment sources were similar during the extreme rainstorm event and during other normal erosive rainfall events. However, grasslands and forests contributed more to the formation of fine material layers, and croplands and bare ground contributed more to the formation of coarse layers, including very coarse layers that mainly included coarse sands and gravels. In the back area of the dam field, cropland contribution to the rainstorm sediment layers was far greater than the bare ground. This indicated a change in erosion patterns caused by the extreme rainstorm. The thick, loose topsoil created by tillage should wash away more easily during extreme rainfall events. Moreover, the change in dominant sediment sources from bare ground and forests in the front area to croplands and bare ground in the back area of the dam field in all deposition layers indicated that bare ground and croplands were highly susceptible to erosion (Wang *et al*., 2016). The high contribution of bare ground and croplands to sediment deposition was closely linked because erosion from bare ground correlated closely to land use types and agricultural activities in croplands, especially unsustainable activities, which contribute greatly to gully erosion (Castilloa & Gómezb, 2016; West *et al*., 2015).

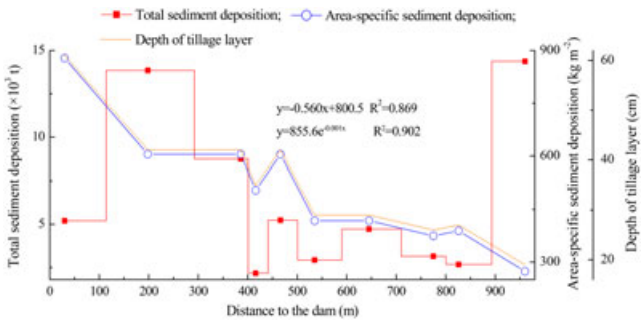

Figure 7. Sediment yield in the tillage layer in the dam field. In the calculation, the mean soil bulk density was 1·44 g cm^{-3}. [Colour figure can be viewed at wileyonlinelibrary.com]

For rainfall events strong enough to produce sediment transport, bare ground were highly erodible throughout such events, while grasslands and forests soil mostly eroded early on, and sediments from both sources were transported close to the dam. In contrast, croplands eroded relatively later during such rainfall events and sediments lagged behind and deposited in the back area of the dam field. This indicated that the erosion sequence in this catchment was determined by the land use type, which was found on plot scale (Chatterjea, 1998). Forest area was mostly created through farmland conversion on slopes steeper than 25 degree under the 'Grain for Green' programme (Tang *et al*., 1998). Artificial forests, dominated by *Robinia pseudoacacia*, have relatively sparse tree crowns and produce relatively little biomass and residue and therefore provided only limited protection against rainfall for the bare ground surface. Thus, the soil in the artificial forest located on steep slopes with little additional vegetation to protect the soil eroded first during the rainfall. The relatively strong erosion on sloping orchards provided evidence for this conclusion (Wang *et al*., 2016). The remaining croplands were located on relatively gentle slopes and were covered by crops during the rainy season. Such dense vegetation cover protected soil against erosion, particularly later in the growing season, and this delayed the start of erosion (Ma *et al*., 2016).

Gullies collapsed easily after absorbing sufficient water from rainfall, and the loose collapsed soil that accumulated on the relative flat bottom of the gullies became highly vulnerable to being transported by runoff or left behind when the carrying capacity of the runoff was exceeded (Yang *et al*., 2006). The soil that was left behind becomes a source of erosion during subsequent rainfalls. Thus, bare ground, mainly gullies, produced sediment throughout rainfall events. This also revealed the significance of gully erosion during the rainstorm (Li *et al*., 2003).

Sediment deposition in layers from the extreme rainstorm event was much greater than sediment deposition in layers from the normal 5-year cumulative rainfall events, and this agrees with the prediction that more severe erosion is produced by extreme rainstorms on the Loess Plateau (Jiao *et al*., 2014). This also indicated the variation in erosion pattern during the extreme rainstorm. Forest, grassland and cropland accounted for 62·2%, 27·1% and 6·9% of the area of the catchment, respectively, and the remaining 3·8% of the area resulted in a gully density of about 2·1 km^{-2}, which is much lower than the average gully density (approximately 8·3 km^{-2}) in the hilly loess areas of northern Shaanxi Province (Tang *et al*., 2015). Despite their relatively low density, these gullies were responsible for a large proportion of the erosion in the catchment. Our observations also suggested that mass wasting (gully collapse and landslides) played an important role on steep hillslopes and exacerbated the effects of strong water flow. This agrees with results from previous research (Canali, 1992; Li *et al*., 2009). Additionally, although sediment particle size became finer along the runoff pathway for both the extreme rainstorm and the normal rainfall events (Schmitter *et al*., 2010), particles during the extreme rainstorm were coarser in comparison that of normal rainfalls manifested the stronger erodibility of the extreme rainstorm.

A study of Chen *et al*. (2016) conducted in the same catchment showed that sediment deposited in the check-dam primarily derived from gullies (which is similar to the bare ground in this study; 34·7%), followed by croplands (28·2%), artificial forests (21·5%), grasslands (12·7%) and fallow lands (2·9%). This analysis was based on composite fingerprint parameters that included Mg, Y, Ti, P, Sc, Co and Cr and achieved a cumulative classification accuracy of 92·2%, which is nearly identical to our result obtained by using fewer parameters under the discriminant analysis (Table V). Compared with their study, the tillage layer that formed before the rainstorm in the present study had a lower sediment contribution from forests (by 9·5 percentage points) and a lower contribution from grasslands (by 5·9 percentage points) but a higher contribution from bare ground (by 17·9 percentage points). This difference mainly derived from changes in vegetation cover. Since 1999, vegetation cover has increased along with the implementation of the 'Grain for Green' programme. Grasslands and forests played a significant role in soil erosion control and led to a decrease in the relative contributions of grasslands and forests to sediment deposition (Wang *et al*., 2016).

CONCLUSIONS

Composite fingerprints allow us to trace sediment sources in a catchment based on sediments deposited in a check-dam during tillage under normal rainfall regimes and above the tillage layer after an extreme rainfall event. For the 626·4 kg m^{-2} of sediment deposited in the dam field after the 2013 extreme rainfall event, most derived from bare ground (44·1% ± 25·5%) and croplands (37·7% ± 35·0%). In both the extreme rainfall layer and the underlying tillage layer, sediment deposition decreased linearly or exponentially with increasing distance from the dam; croplands and bare ground were the primary sediment sources. The magnitude of the sediment deposition during the extreme rainstorm was much greater than the normal 5-year cumulative sediment deposition in the tillage layers. Croplands and bare ground contributed all deposition in the rainstorm event layer at the back area of the dam field, whereas grasslands and forests contributed to the upper layers in the front and middle areas. These results provide evidence of the severe erosion caused by the extreme rainstorm events and reveal the variations in its source patterns. Gully collapses and landslides were significant contributors to soil erosion patterns in the catchment. It is obvious that check-dam played an important role in sediment interception and that the 'Grain for Green' programme also had a significant effect. Damaged check-dam should therefore be repaired for purposes of soil and water conservation of catchments, and new check-dam should be established at locations where existing ones have been neutralized by sediments.

ACKNOWLEDGEMENTS

This study was financially supported by the National Natural Science Foundation of China (41671281), the Special Fund for Basic Scientific Research of the Northwest A&F University of China of Ministry of Education (grant no 2452015095), the Special Funds of Scientific Research Programs of the State Key Laboratory of Soil Erosion and Dryland Farming on the Loess Plateau of Ministry of Science and Technology (A314021403-C2) and the National Key Research and Development Program of China of Ministry of Science and Technology (2016YFC0402406). The authors sincerely appreciate Dr Geoffrey Hart and Dr Brian Doonan for their English language editing. Finally, the authors also gratefully acknowledge four anonymous referees for their valuable comments that led to the improvement of this manuscript.

REFERENCES

Bird A, Stevens T, Rittner M, Vermeesch P, Carter A, Andò S, Garzanti E, Lu HY, Nie JS, Lin Z, Zhang HZ, Xu ZW. 2015. Quaternary dust source variation across the Chinese Loess Plateau. *Palaeogeography Palaeoclimatology Palaeoecology* **435**: 254–264. https://doi.org/10.1016/j.palaeo.2015.06.024.

Boardman J, Foster IDL, Dearing JA. 1990. *Soil erosion on agricultural land*. John Wiley and Sons: Chichester.

Brevik EC, Cerdà A, Mataix-Solera J, Pereg L, Quinton JN, Six J, Van Oost K. 2015. The interdisciplinary nature of SOIL. *The Soil* **1**: 117–129. https://doi.org/10.5194/soil-1-117-2015.

Canali GE. 1992. The impact of watershed dynamics and homogeneity on sedimentation. Ph.D. dissertation, Colorado State University.

Cao JJ, Chow JC, Watson JG, Wu F, Han YM, Jin ZD, Shen ZX, An ZS. 2008. Size-differentiated source profiles for fugitive dust in the Chinese Loess Plateau. *Atmospheric Environment* **42**: 2,261–2,275. https://doi.org/10.1016/j.atmosenv.2007.12.041.

Castilloa C, Gómezb JA. 2016. A century of gully erosion research: urgency, complexity and study approaches. *Earth Science Reviews* **160**: 300–319. https://doi.org/10.1016/j.earscirev.2016.07.009.

Chaparro MAE, Krishnamoorthy N, Chaparro MAE, Lecomte KL, Mullainathan S, Mehra R, Sinito AM. 2015. Magnetic, chemical and radionuclide studies of river sediments and their variation with different physiographic regions of Bharathapuzha river, southwestern India. *Studia Geophysica et Geodaetica* **59**: 438–460. https://doi.org/10.1007/s11200-014-0145-6.

Chatterjea K. 1998. The impact of tropical rainstorms on sediment and runoff generation from bare and grass-covered surfaces: a plot study from Singapore. *Land Degrad. Develop.* **9**: 143–157. https://doi.org/10.1002/(SICI)1099-145X(199803/04)9:2<143::AID-LDR264>3.0.CO;2-I.

Chen FX, Zhang FB, Fang NF, Shi ZH. 2016. Sediment source analysis using the fingerprinting method in a small catchment of the Loess Plateau. China. *J. Soils Sed.* **16**: 1,655–1,669. https://doi.org/10.1007/s11368-015-1336-7.

China Meteorological Administration. 2012. National precipitation grade standard of China (GB/T 28592-2012).

Collins AL, Pulley S, Foster IDL, Gellis A, Porto P, Horowitz AJ. 2016. Sediment source fingerprinting as an aid to catchment management: a review of the current state of knowledge and a methodological decision-tree for end-users. *Journal of Environmental Management*. https://doi.org/10.1016/j.jenvman.2016.09.075.

Collins AL, Walling DE. 2002. Selecting fingerprint properties for discriminating potential suspended sediment sources in river basins. *Journal of Hydrology* **261**: 218–244. https://doi.org/10.1016/S0022-1694(02)00011-2.

Collins AL, Walling DE. 2004. Documenting catchment suspended sediment sources: problems, approaches and prospects. *Progr. Phys. Geogr.* **28**: 159–196. https://doi.org/10.1191/0309133304pp409ra.

Collins AL, Walling DE, Leeks GJL. 1997. Source type ascription for fluvial suspended sediment based on a quantitative composite fingerprinting technique. *Catena* **29**: 1–27. https://doi.org/10.1016/S0341-8162(96)00064-1.

Ding ZL, Yang SL, Liu TS, Sun JM. 2001. Geochemistry of the Pliocene red clay formation in the Chinese Loess Plateau and implications for its origin, source provenance and paleoclimate change. *Geochimica et Cosmochimica Acta* **65**: 901–913. https://doi.org/10.1016/S0016-7037(00)00571-8.

Du L, Li WG, Wu LR. 2014. Causes and meteorological services of rainstorm disasters in July 2013 in Yan'an. *J. Anhui Agric. Sci.* **42**: 11,437–11,439 (in Chinese with English abstract).

Durán-Zuazoa VH, Francia-Martínez JR, García-Tejero I, Tavira SC. 2013. Implications of land-cover types for soil erosion on semiarid mountain slopes: towards sustainable land use in problematic landscapes. *Acta Ecologica Sinica* **33**: 272–281. https://doi.org/10.1016/j.chnaes.2013.07.007.

Gellis AC, Walling DE. 2013. Sediment source fingerprinting (tracing) and sediment budgets as tools in targeting river and watershed restoration programs. In *Stream restoration in dynamic fluvial systems: scientific approaches, analyses, and tools*, Vol. **194**, Simon A, Bennett SJ, Castro JM (eds). Geophysical Monograph Series: Washington; 263–291. http://doi.10.1029/2010GM000960

Grousset FE, Biscaye PE. 2005. Tracing dust sources and transport patterns using Sr. *Nd and Pb isotopes Chemical Geology* **222**: 149–167. https://doi.org/10.1016/j.chemgeo.2005.05.006.

Guzmán G, Quinton JN, Nearing MA, Mabit L, Gómez JA. 2013. Sediment tracers in water erosion studies: current approaches and challenges. *J. Soils Sed.* **13**: 816–833. https://doi.org/10.1007/s11368-013-0659-5.

Haddadchi A, Olley J, Laceby P. 2014. Accuracy of mixing models in predicting sediment source contributions. *Sci. Total Environ.* **497-498**: 139–152. https://doi.org/10.1016/j.scitotenv.2014.07.105.

Haddadchi A, Ryder DS, Eveard O, Olley J. 2013. Sediment fingerprinting in fluvial systems: review of tracers, sediment sources and mixing models. *Intern. J. Sediment Res.* **28**: 560–578. https://doi.org/10.1016/S1001-6279(14)60013-5.

He T, Chen Y, Balsam W, Qiang XK, Liu LW, Chen J, Ji JF. 2013. Carbonate leaching processes in the red clay formation, Chinese Loess Plateau: fingerprinting East Asian summer monsoon variability during the late Miocene and Pliocene. *Geophysical Research Letters* **40**: 194–198. https://doi.org/10.1029/2012GL053786.

Huang YH, Wu WY, Feng W, Li ZG. 2014. Main types and characteristics of the geo-hazards triggered by heavy rain on July 3 in Yan'an. *Shaanxi. Northwest. Geology.* **47**: 140–146.

Huisman LHN, Karthikeyan KG, Lamba J, Thompson AM, Peaslee G. 2013. Quantification of seasonal sediment and phosphorus transport dynamics in an agricultural watershed using radiometric fingerprinting techniques. *J. Soils Sed.* **13**: 1,724–1,734. https://doi.org/10.1007/s11368-013-0769-0.

Jia XP, Wang HB, Xiao JH. 2011. Geochemical elements characteristics and sources of the riverbed sediment in the yellow river's desert channel. *Environment and Earth Science* **64**: 2,159–2,173. https://doi.org/10.1007/s12665-011-1044-6.

Jiao J, Wang Z, Zhao G, Wang W, Mu X. 2014. Changes in sediment discharge in a sediment-rich region of the Yellow River from 1955 to 2010: implications for further soil erosion control. *Journal of Arid Land* **6**: 540–549. https://doi.org/10.1007/s40333-014-0006-8.

Kinnell PIA. 2013. Modeling of the effect of flow depth on sediment discharged by rain-impacted flows from sheet and interrill erosion areas: a review. *Hydrol. Proc.* **27**: 2,567–2,578. https://doi.org/10.1002/hyp.9363.

Koiter AJ, Owens PN, Petticrew EL, Lobb DA. 2013. The behavioural characteristics of sediment properties and their implications for sediment fingerprinting as an approach for identifying sediment sources in river basins. *Earth-Sci. Reviews.* **125**: 24–42. https://doi.org/10.1016/j.earscirev.2013.05.009.

Li TJ, Wang GQ, Huang YF, Fu XD. 2009. Modeling the process of hillslope soil erosion in the Loess Plateau. *J. Environ. Inform.* **14**: 1–10. https://doi.org/10.3808/jei.200900148.

Li XG, Wei X. 2014. Analysis of the relationship between soil erosion risk and surplus floodwater during flood season. *Journal of Hydrologic Engineering* **19**: 1,294–1,311. https://doi.org/10.1061/(ASCE)HE.1943-5584.0000912.

Li XG, Wei X, Wei N. 2016. Correlating check dam sedimentation and rainstorm characteristics on the Loess Plateau, China. *Geomorphology* **265**: 84–97. https://doi.org/10.1016/j.geomorph.2016.04.017.

Li Y, Poesen J, Yang JC, Fu B, Zhang JH. 2003. Evaluating gully erosion using ^{137}Cs and ^{210}Pb/^{137}Cs ratio in a reservoir catchment. *Soil Till. Res.* **69**: 107–115. https://doi.org/10.1016/S0167-1987(02)00132-0.

Li YJ, Jiao JY, Wang ZJ, Cao BT, Wei YH, Hu S. 2016. Effects of revegetation on soil organic carbon storage and erosion-induced carbon loss under extreme rainstorms in the hill and gully region of the Loess Plateau. *International Journal of Environmental Research and Public Health* **13**: 456. https://doi.org/10.3390/ijerph13050456.

Long Y, Zhang XB, Wen AB, He XB. 2012. ^{137}Cs fingerprinting technique for erosion and sedimentation studies. *Journal of Mountain Science* **9**: 34–40. https://doi.org/10.1007/s11629-012-2203-2.

López-Vicente M, Quijano L, Palazón L, Gaspar L, Navas A. 2015. Assessment of soil redistribution at catchment scale by coupling a soil erosion model and a sediment connectivity index (central Spanish Pre-Pyrenees). *Cuad. Investig. Geogr.* **41**: 127–147. https://doi.org/10.18172/cig.2649.

Ma B, Li CD, Li ZB, Wu FQ. 2016. Effects of crops on runoff and soil loss on sloping farmland under simulated rainfall. *CLEAN-Soil, Air, Water* **44**: 849–857. https://doi.org/10.1002/clen.201400241.

McKinley R, Radcliffe D, Mukundan R. 2013. A streamlined approach for sediment source fingerprinting in a Southern Piedmont watershed, USA. *Journal of Soils and Sediments* **13**: 1,754–1,769. https://doi.org/10.1007/s11368-013-0723-1.

Ministry of Water Resources, China, 2013. Bulletin of first national water census for soil and water conservation. Ministry of Water Resources, Beijing, 1–6. (in Chinese without English abstract)

Nosrati K. 2016. Ascribing soil erosion of hillslope components to river sediment yield. *Journal of Environmental Management* . https://doi.org/10.1016/j.jenvman.2016.10.011.

Palazón L, Latorre B, Gaspar L, Blake WH, Smith HG, Navas A. 2015. Comparing catchment sediment fingerprinting procedures using an auto-evaluation approach with virtual sample mixtures. *Sci. Total Environ.* **532**: 456–466. https://doi.org/10.1016/j.scitotenv.2015.05.003.

Reiffarth DG, Petticrew EL, Owens PN, Lobb DA. 2016. Sources of variability in fatty acid (FA) biomarkers in the application of compound-specific stable isotopes (CSSIs) to soil and sediment fingerprinting and tracing: a review. *Sci. Total Environ.* **565**: 8–27. https://doi.org/10.1016/j.scitotenv.2016.04.137.

Renard KG, Yoder DC, Lightle DT, Dabney SM. 2011. Universal soil loss equation and revised universal soil loss equation. In: Morgen RPC, Nearing MA (eds.) *Handbook of erosion modelling*, Blackwell Publishing Ltd. 137–167.

Schmitter P, Dercon G, Hilger T, Thi Le Ha T, Huu Thanh N, Lam N, Duc Vien T, Cadisch G. 2010. Sediment induced soil spatial variation in paddy fields of Northwest Vietnam. *Geoderma* **155**: 298–307. https://doi.org/10.1016/j.geoderma.2009.12.014.

Silva-Filho EV, Sanders CJ, Bernat M, Figueiredo AMG, Sella SM, Wasserman J. 2011. Origin of rare earth element anomalies in mangrove sediments, Sepetiba Bay, SE Brazil: used as geochemical tracers of sediment sources. *Environment and Earth Science* **64**: 1,257–1,267. https://doi.org/10.1007/s12665-011-0942-y.

Smith P, Cotrufo MF, Rumpel C, Paustian K, Kuikman PJ, Elliott JA, McDowell R, Griffiths RI, Asakawa S, Bustamante M, House JI, Sobocká J, Harper R, Pan G, West PC, Gerber JS, Clark JM, Adhya T, Scholes RJ, Scholes MC. 2015. Biogeochemical cycles and biodiversity as key drivers of ecosystem services provided by soils. *The Soil* **1**: 665–685. https://doi.org/10.5194/soild-2-537-2015.

Sukhija BS, Reddy DV, Nagabhushanam P. 1998. Isotopic fingerprints of paleoclimates during the last 30,000 years in deep confined ground waters of southern India. *Quaternary Research* **50**: 252–260. https://doi.org/10.1006/qres.1998.2001.

Sun LY, Fang HY, Qi DL, Li JL, Cai QG. 2013. A review on rill erosion process and its influencing factors. *Chinese Geogr. Sci.* **23**: 389–402. https://doi.org/10.1007/s11769-013-0612-y.

Taguas EV, Guzmán E, Guzmán G, Vanwalleghem T, Gómez JA. 2015. Characteristics and importance of rill and gully erosion: a case study in a small catchment of a marginal olive grove. *Cuad. Investig. Geogr.* **41**: 107–126. https://doi.org/10.18172/cig.2644.

Tang GA, Song XD, Li FY, Zhang Y. 2015. Slope spectrum critical area and its spatial variation in the Loess Plateau of China. *Journal of Geographical Sciences* **25**: 1,452–1,466. https://doi.org/10.1007/s11442-015-1245-0.

Tang KL, Zhang KL, Lei AL. 1998. Critical slope gradient for compulsory abandonment of farmland on the hilly Loess Plateau. *Chinese Science Bulletin* **43**: 409–412. https://doi.org/10.1007/BF02883721.

USDA, 1951. United States Department of Agriculture (USDA) soil survey manual. USDA Washington DC. Handbook No. 18.

USDA, 1996. Wind Erosion Prediction System (WEPS) technical documentation. United States Department of Agriculture, Agricultural Research Service, Wind Erosion Research Unit, Manhattan, Kansas, USA.

Verheijen FGA, Jones RJA, Rickson RJ, Smith CJ. 2009. Tolerable versus actual soil erosion rates in Europe. *Earth Science Reviews* **94**: 23–38. https://doi.org/10.1016/j.earscirev.2009.02.003.

Viparelli E, Lauer JW, Belmont P, Parker G. 2013. A numerical model to develop long-term sediment budgets using isotopic sediment fingerprints. *Computational Geosciences* **53**: 114–122. https://doi.org/10.1016/j.cageo.2011.10.003.

Walling DE. 2005. Tracing suspended sediment sources in catchments and river systems. *Sci. Total Environ.* **344**: 159–184. https://doi.org/10.1016/j.scitotenv.2005.02.011.

Walling DE, Owens PN, Leeks GJL. 1999. Fingerprinting suspended sediment sources in the catchment of the River Ouse, Yorkshire, UK. *Hydrol. Proc.* **13**: 955–975. https://doi.org/10.1002/(SICI)1099-1085.

Wang S, Fu BJ, Piao SL, Lü YH, Ciais P, Feng XM. 2016. Reduced sediment transport in the Yellow River due to anthropogenic changes. *Nature Geoscience* **9**: 38–41. https://doi.org/10.1038/ngeo2602.

Wang ZJ, Jiao JY, Rayburg S, Wang QL, Su Y. 2016. Soil erosion resistance of "Grain for Green" vegetation types under extreme rainfall conditions on the Loess Plateau, China. *Catena* **141**: 109–116. https://doi.org/10.1016/j.catena.2016.02.025.

Warren N, Allan IJ, Carter JE, House WA, Parker A. 2003. Pesticides and other micro-organic contaminants in freshwater sedimentary environments-a review. *Applied Geochemistry* **18**: 159–194. https://doi.org/10.1016/S0883-2927(02)00159-2.

Watson EB, Pasternack GB, Gray AB, Goñi M, Woolfolk AM. 2013. Particle size characterization of historic sediment deposition from a closed estuarine lagoon. *Central California. Estuarine Coast. Shelf Sci.* **126**: 23–33. https://doi.org/10.1016/j.ecss.2013.04.006.

Wei YH, He Z, Li YJ, Jiao JY, Zhao GJ, Mu XM. 2017. Sediment yield deduction from check-dams deposition in the weathered sandstone watershed on the north Loess Plateau. *China. Land Degrad. Develop.* **28**: 217–231. https://doi.org/10.1002/ldr.2628.

West AJ, Arnold M, Aumaître G, Bourlès DL, Keddadouche K, Bickle M, Ojha T. 2015. High natural erosion rates are the backdrop for present-day soil erosion in the agricultural Middle Hills of Nepal. *Earth Surf. Dynam.* **3**: 363–387. https://doi.org/10.5194/esurf-3-363-2015.

Xu LJ, 2008. Study on the composite fingerprinting flood suspended sediment sources in the catchment on the Loess Plateau. Master Dissertation of Graduate University of Chinese Academy of Science.

Xu XX, Ju TJ, Zheng SQ. 2013. Sediment sources of Yan'gou watershed in the Loess Hilly region China under a certain rainstorm event. *Springer Plus* **2**: S2. http://www.springerplus.com/content/2/S1/S2

Yang MY, Tian JL, Liu PL. 2006. Investigating the spatial distribution of soil erosion and deposition in a small catchment. *Soil and Till. Res.* **87**: 186–193. https://doi.org/10.1016/j.still.2005.03.010.

Zhang HY, Shi ZH, Fang NF, Guo MH. 2015. Linking watershed geomorphic characteristics to sediment yield: evidence from the Loess Plateau of China. *Geomorphology* **234**: 19–27. https://doi.org/10.1016/j.geomorph.2015.01.014.

Zhao GJ, Klik A, Mu XM, Wang F, Gao P, Sun WY. 2015. Sediment yield estimation in a small watershed on the northern Loess Plateau, China. *Geomorphology* **241**: 343–352. https://doi.org/10.1016/j.geomorph.2015.04.020.

Zhao GJ, Yue XL, Tian P, Mu XM, Xu WL, Wang F, Gao P, Sun WY. 2016. Comparison of the suspended sediment dynamics in two Loess Plateau catchments. *China. Land Degrad. Develop.* https://doi.org/10.1002/ldr.2645.

Zheng MG, Cai QG, Cheng QJ. 2008. Modelling the runoff-sediment yield relationship using a proportional function in hilly areas of the Loess Plateau, North China. *Geomorphology* **93**: 288–301. https://doi.org/10.1016/j.geomorph.2007.03.001.

Zheng MG, Qin F, Yang JS, Cai QG. 2013. The spatio-temporal invariability of sediment concentration and the flow–sediment relationship for hilly areas of the Chinese Loess Plateau. *Catena* **109**: 164–176. https://doi.org/10.1016/j.catena.2013.03.017.

Zhou PH, Wang ZL. 1992. A study on rainstorm causing soil erosion in the Loess Plateau. *Journal of Soil and Water Conservation* **6**: 1–5 (in Chinese with English abstract).